Gastroenterology 2024;166:667–679

Cholangiocytes Modulate CD100 Expression in the Liver and Facilitate Pathogenic T-Helper 17 Cell Differentiation

Xiaojun Jiang,[1,2] Kari Otterdal,[2] Brian K. Chung,[1,2,3] Christopher Maucourant,[4] Jørgen D. Rønneberg,[1,2,3] Christine L. Zimmer,[4] Jonas Øgaard,[1,2] Yuliia Boichuk,[1,2] Sverre Holm,[2] Daniel Geanon,[4] Georg Schneditz,[1,2] Annika Bergquist,[5] Niklas K. Björkström,[4] and Espen Melum[1,2,3,6,7]

[1]Norwegian PSC Research Center, Division of Surgery, Inflammatory Diseases and Transplantation, Oslo University Hospital Rikshospitalet, Oslo, Norway; [2]Research Institute of Internal Medicine, Division of Surgery, Inflammatory Diseases and Transplantation, Oslo University Hospital Rikshospitalet, Oslo, Norway; [3]Institute of Clinical Medicine, Faculty of Medicine, University of Oslo, Oslo, Norway; [4]Center for Infectious Medicine, Department of Medicine Huddinge, Karolinska Institutet, Karolinska University Hospital, Stockholm, Sweden; [5]Department of Gastroenterology and Hepatology, Karolinska University Hospital Huddinge, Karolinska Institutet, Stockholm, Sweden; [6]Section of Gastroenterology, Department of Transplantation Medicine, Division of Surgery, Inflammatory Diseases and Transplantation, Oslo University Hospital Rikshospitalet, Oslo, Norway; and [7]Hybrid Technology Hub-Centre of Excellence, Institute of Basic Medical Sciences, Faculty of Medicine, University of Oslo, Oslo, Norway

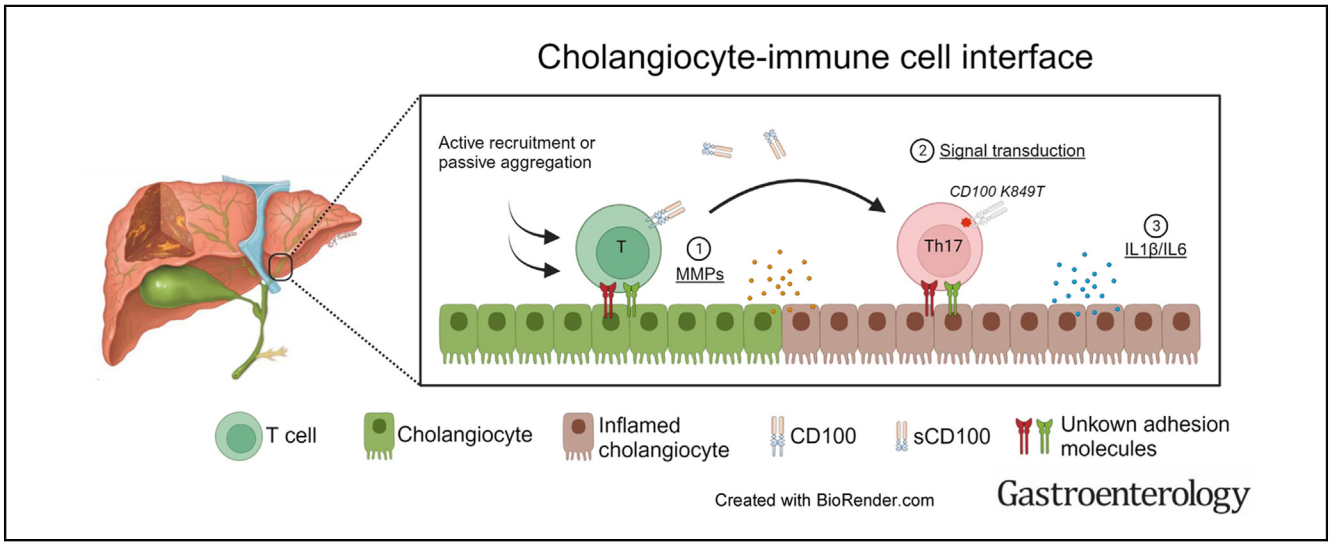

BACKGROUND & AIMS: Chronic inflammation surrounding bile ducts contributes to the disease pathogenesis of most cholangiopathies. Poor efficacy of immunosuppression in these conditions suggests biliary-specific pathologic principles. Here we performed biliary niche specific functional interpretation of a causal mutation (CD100 K849T) of primary sclerosing cholangitis (PSC) to understand related pathogenic mechanisms. **METHODS:** Biopsy specimens of explanted livers and endoscopy-guided sampling were used to assess the CD100 expression by spatial transcriptomics, immune imaging, and high-dimensional flow cytometry. To model pathogenic cholangiocyte-immune cell interaction, splenocytes from mutation-specific mice were cocultured with cholangiocytes. Pathogenic pathways were pinpointed by RNA sequencing analysis of cocultured cells and cross-validated in patient materials. **RESULTS:** CD100 is mainly expressed by immune cells in the liver and shows a unique pattern around PSC bile ducts with RNA-level colocalization but poor detection at the protein level. This appears to be due to CD100 cleavage as soluble CD100 is increased. Immunophenotyping suggests biliary-infiltrating T cells as the major source of soluble CD100, which is further supported by reduced surface CD100 on T cells and increased metalloproteinases in cholangiocytes after coculturing. Pathogenic T cells that adhered to cholangiocytes up-regulated genes in the T-helper 17 cell differentiation pathway, and the CD100 mutation boosted this process. Consistently, T-helper 17 cells dominate biliary-resident CD4 T cells in patients. **CONCLUSIONS:** CD100 exerts its functional impact through cholangiocyte-immune cell cross talk and underscores an active, proinflammatory role of cholangiocytes that can be relevant to novel treatment approaches.

Keywords: Biliary Inflammatory Disease; PSC Pathogenesis; SEMA4D/CD100; PSC Causal Mutation.

Understanding the function of causal genes underlying monogenic disorders that lead to chronic inflammation in specific organs can unravel mechanisms involved in tissue-specific pathogenic immune processes. Mechanisms revealed from 1 causal gene may also contribute to common, complex diseases with similar clinical manifestations, as seen for Alzheimer's disease and cancers.[1,2] We have previously identified CD100 K849T as the causal mutation in a familial subtype of primary sclerosing cholangitis (PSC),[3] a severe liver disease without approved medical treatments characterized by progressive chronic biliary inflammation leading to liver cirrhosis, cholangiocarcinoma development, and a need for liver transplantation.[4–6] This gain-of-function mutation is located at the intracellular tail of CD100, also known as semaphorin 4D (SEMA4D), with a direct impact on the function of CD100-expressing cells, most notably the cytokine production of T cells.[3]

Despite the broad expression of CD100 and its receptors (CD72 and plexin B1/B2) in various organs, patients carrying the mutation develop no systemic immune disorders but exhibit a classical PSC phenotype with variable manifestations of site-restricted immune dysregulations (ie, inflammatory bowel disease and autoimmune hepatitis), with the only shared phenotype being bile duct inflammation. This striking human observation raises the possibility that CD100 plays a unique role in the liver or biliary, or both, local immunity contributing to PSC pathogenesis in patients with the mutation. Similar mechanisms or closely related phenotypes are probably also present in patients not carrying the pathogenic mutation.

The current understanding of CD100 function is focused on facilitation of general immune activities with limited data on tissue-specific roles.[7–9] CD100 is a transmembrane semaphorin protein originally identified in activated T cells[10] and later found to be constitutively expressed by diverse immune cells and involved in assembly of immunologic synapses.[7,11] It triggers reciprocal signals to both receptor- and CD100-expressing cells, promoting antigen presentation and immune cell maturation, activation, and migration.[8]

Importantly, CD100 acts as a costimulatory molecule transducing T-cell activation signaling through the cytoplasmic tail,[12] where the PSC causal K849T mutation is located. Specialized metalloproteinases (MMPs), such as a disintegrin and metalloproteinase domain-containing protein (ADAM) 10, ADAM17, ADAM metallopeptidase with thrombospondin type 1 motif (ADAMTS4), MMP8, and MMP14,[9] cleave the extracellular domain of CD100 to yield a soluble form (sCD100)[8] that displays proinflammatory activity in autoimmune diseases.[13–16]

The present study was conducted to determine the liver- or biliary-specific, or both, functional involvement of CD100 and how the CD100 mutation contributes to initiating or amplifying bile duct-damaging immune responses. To that end, we carefully examined CD100 expression in liver tissue sections from explanted PSC livers and specifically compared immune cells infiltrating bile ducts against those in paired blood samples. Then, we modeled the interaction of CD100 mutant and wild-type (WT) immune cells with cholangiocytes, the epithelial cells lining the bile ducts, to establish key pathogenic immune features. Finally, we validated the findings obtained in the murine system in material collected from patients.

WHAT YOU NEED TO KNOW

BACKGROUND AND CONTEXT

A SEMA4D/CD100 mutation has been identified as a causal mutation for a Mendelian form of primary sclerosing cholangitis. It is largely unknown how this mutation contributes to localized biliary inflammation.

NEW FINDINGS

CD100 is involved in cholangiocyte-immune cell cross talk, and the CD100 mutation enhances pathogenic T-helper 17 cell differentiation.

LIMITATIONS

The specific signaling pathway through which the CD100 mutation impacts T-helper 17 differentiation at the cholangiocyte-immune cell interface remains to be defined.

CLINICAL RESEARCH RELEVANCE

Our findings establish a link between the CD100 mutation and biliary inflammation, highlighting the utility of using mutation-specific tools for identification of key molecules central to primary sclerosing cholangitis pathogenesis that can represent potential treatment targets for biliary inflammation.

BASIC RESEARCH RELEVANCE

We have identified important biliary-specific cellular players and a pathogenic process that CD100 is involved in. We also suggest a distinct and complementary mechanism in which T-helper 17 cells are locally differentiated due to their interaction with cholangiocytes.

Materials and Methods

Ethics Approval

This study was approved by the Regional Ethical Committee in Norway (S-08872b; 2012-286) and the Regional Ethical Review Board in Stockholm, Sweden (2013/1449-31/4). The

Abbreviations used in this paper: **CD, cluster of differentiation; CFSE, carboxyfluorescein succinimidyl ester; CK19, cytokeratin 19; DCM, dead cell marker; ERCP, endoscopic retrograde cholangiopancreatography; IL, interleukin; MMPs, metalloproteinases; PBC, primary biliary cholangitis; PBMCs, peripheral blood mononuclear cells; PSC, primary sclerosing cholangitis; RORγt, retinoic acid-related orphan receptor-γ; sCD100, soluble cluster of differentiation 100; SEMA4D, semaphorin 4D; TEM, effector memory T cells; Th17, T-helper 17 cells; UMAP, Uniform Manifold Approximation and Projection analysis; WT, wild-type.**

Most current article

0016-5085
https://doi.org/10.1053/j.gastro.2023.11.283

guidelines of the Declaration of Helsinki were followed. Written informed consent was provided by all participants. Protocols for animal experiments were approved by Mattilsynet, Norway (FOTS 22988) and followed all recommendations from the Federation of European Laboratory Animal Science Associations.

Human Materials

Human liver biopsy specimens were collected after liver transplantation at Oslo University Hospital, Oslo, Norway. Serum, plasma, and bile samples from patients who received a transplant and controls were also collected at Oslo University Hospital. Brush cytology was obtained during endoscopic retrograde cholangiopancreatography (ERCP) at Karolinska University Hospital, Karolinska, Sweden. Clinical characteristics of patients are presented in Supplementary Table 1.

Mice

C57BL/6 mice with homologous CD100 K849T mutation have been described.[3] WT and CD100-mutated mice (sibling littermates) were bred in-house and maintained under specific pathogen-free conditions at the Department of Comparative Medicine, Institute of Basic Medical Sciences, University of Oslo. Male or female mice (8–10 weeks old) were used.

Isolation of Murine Primary Cholangiocytes and Splenocytes

The portal vein was cannulated, and the liver was perfused with Liver Perfusion Medium (Thermo Fisher Scientific), followed by 0.5 mg/mL collagenase I (Sigma-Aldrich). The biliary trees were cleaned by washing away hepatocytes, cut into small pieces, and incubated for 1 hour with 0.5 mg/mL collagenase I, 0.1 mg/mL deoxyribonuclease I (Sigma-Aldrich), and 1 mg/mL Pronase E (Santa Cruz Biotechnology) at 37°C. Samples were filtered and washed twice. Cells were then seeded in 1 mg/mL collagen I hydrogel (Corning) or Matrigel (Corning) with a murine version of cholangiocyte expansion medium.[17] After 2 weeks, cell purity was examined by flow cytometry. Splenocytes were isolated by forcing the spleen through 70-μm nylon mesh and subsequent erythrocyte lysing.

Cell Lines

Small and large cholangiocytes were SV40 large T antigen–immortalized murine cell lines.[18] Both lines were maintained in Gibco Dulbecco's modified Eagle medium with high glucose supplemented with fetal calf serum and 1% Gibco Antibiotic-Antimycotic (Thermo Fisher Scientific), and used for coculture experiments.

Spatial Transcriptome Data Analysis

Spatial transcriptome analysis was performed on previously published 10× Visium data[19] that included liver samples from PSC (n = 4) and non-PSC controls with primary biliary cholangitis (PBC; n = 2) or alcoholic liver disease (n = 2). A total of 9206 transcriptomics profiles were generated for RNA capture spots and aligned with corresponding H&E images. *SEMA4D* was used to define $CD100^+$ regions and *KRT19* for cytokeratin 19^+ ($CK19^+$) cholangiocytes using Loupe Browser software (10× Genomics). Similarly, *CD3D* was used as a marker for T cells and *TPSAB1* for mast cells.

Immunohistochemistry

Sequential sections were cut from formalin-fixed, paraffin-embedded liver blocks (6 PSC and 4 PBC) at a thickness of 5 μm and stained with rabbit anti-CD100 (1:100; Abcam) and rabbit anti-CD3 (1:100; Dako), respectively, following a standard immunohistochemistry protocol provided by Dako. Two to 3 photomicrographs of diseased bile duct areas (×100) were randomly taken from each slide and analyzed by Fiji software.[20]

Immunofluorescence

Immunofluorescence was performed on extra sections adjacent to the section used for spatial transcriptome analysis. Each sections were stained with appropriate antibodies (Supplementary Table 2) for CD100, cholangiocytes, T cells, and mast cells according to established protocols.[21] Stained slides were scanned by ZEISS Axio Scan.Z1 Slide Scanner (Carl Zeiss AG) and analyzed by Zen 2.6 (blue edition) or QuPath 0.4.3.

Enzyme-linked Immunosorbent Assay

Soluble CD100/SEMA4D levels were measured with the Human Semaphorin 4D ELISA Kit (Thermo Fisher Scientific). Matched serum, plasma, and bile samples from the same individual were examined when available (24 PSC, 11 non-PSC disease controls, 23 healthy donors). Bile was directly collected from the gallbladder of patients after liver transplantation.

Flow Cytometry of Human Samples

Biliary immune cells were collected from ERCP brush cytology, as described previously.[21] Peripheral blood mononuclear cells (PBMCs) or biliary immune cells were stained for cell surface markers and dead cell marker (DCM) (Supplementary Table 3). For intracellular staining, cells were fixed and permeabilized using the Foxp3/Transcription Factor Staining Buffer Set (eBioscience). Samples were acquired on a BD Symphony A5 (BD Biosciences) flow cytometer, and the data were analyzed by FlowJo 10 (BD Biosciences). For uniform manifold approximation and projection (UMAP) analysis,[22] manually gated populations were exported from FlowJo and analyzed in Python 3.8.8. The umap-learn 0.5.3 (https://doi.org/10.48550/arXiv.1802.03426) package was used for executing the UMAP algorithm, and the resulting UMAP *x* and *y* coordinates were plotted with Matplotlib 3.6.3 (https://matplotlib.org/3.6.3/) and seaborn 0.12.2 (https://seaborn.pydata.org/).

Coculture Experiment

Small or large cholangiocytes (1×10^5) were seeded into 24-well plates at day 0. Splenocytes (1×10^6) were added into the culture on day 1 after cholangiocytes were labeled with 5 μmol/L carboxyfluorescein succinimidyl ester (CFSE; Thermo Fisher Scientific). For experiments with primary cholangiocytes, 1×10^5 cells (passage 4–7, purity >90%) were seeded (day 0) into 24-well collagen I-coated plates (Thermo Fisher Scientific). Splenocytes were added at day 3 when primary cells reached 90% confluence. Anti-CD3 (clone 145-2C11; BioLegend) and anti-CD28 (clone 37.51; BioLegend) were added subsequently at a final concentration of 2 μg/mL. Alternatively, BD Leukocyte Activation Cocktail (BD Biosciences) containing phorbol myristate acetate and ionomycin

was used for stimulation. The cells in the suspension or adherent layer were collected separately on day 2. For cytokine detection, BD stop and plug (BD Biosciences) were added 4 hours before harvest.

Flow Cytometry of Mouse Sample

Cells collected after coculture were incubated with anti-mouse CD16/32 (BioLegend) to block Fc receptors and stained (Supplementary Table 3). CellEvent Senescence Green Kit (Thermo Fisher Scientific) was used for assessment of senescence. Samples were acquired on BD Symphony A5 or LSRFortessa (BD Biosciences) flow cytometer and analysis was performed as for the human samples.

Bulk RNA Sequencing and Data Analysis

After coculture, live T cells ($DCM^-CFSE^-CD3^+$) and large cholangiocytes (DCM^-CFSE^+) were purified by BD FACSAria II (BD Biosciences), snap frozen, and delivered to Novogene for RNA isolation and sequencing. All samples had 2 to 3 biological replicates and were sequenced by the NovaSeq 6000 system (Illumina) in paired-end 150 base pair (PE150) mode. Raw reads were filtered and mapped to the reference genome (*Mus musculus* [Genome Reference Consortium Mouse Build 38 {GRCm38/mm10}]). The DESeq2 R package (Bioconductor)[23] was used for differential expression analysis. The clusterProfiler[24] software was used for enrichment analysis.

Statistical Analysis

If not otherwise stated, statistical analysis was performed using GraphPad Prism (GraphPad Prism Software). The distributions of data were evaluated by normality and lognormality tests. When normally distributed, comparisons between 2 groups were performed by 2-tailed paired or unpaired *t* tests. Otherwise, comparisons were performed by 2-tailed nonparametric Mann-Whitney or Wilcoxon's matched-pairs tests. For comparisons with 3 groups, 1-way analysis of variance was used, followed by Bonferroni's correction. Differences were considered statistically significant when $P < .05$.

Results

Unexpected CD100 Expression Pattern Around the Bile Ducts

CD100 is clearly present in all organs in the human body (Supplementary Figure 1*A*) reported in the Human Protein Atlas (https://www.proteinatlas.org/) although with a low expression in the liver at a messenger RNA level (Supplementary Figure 1*B*). This fact can be due to the absent or very low level of CD100 in hepatocytes and cholangiocytes (Supplementary Figure 1*C*), 2 cell types abundantly present in the liver.[25] By contrast, a high expression of CD100 was observed in hepatic immune cells, such as T, B, and Kupffer cells (Supplementary Figure 1*C*), supporting the notion that the main actions of CD100 in the liver are exerted through the immune system.

To quantify and localize CD100 specifically in PSC livers, we interrogated our in-house spatial transcriptomics data.[19] The proportion of $CD100^+$ (*SEMA4D*$^+$) regions detected in PSC (n = 4) and non-PSC livers (n = 4) were comparable, and the read counts of *SEMA4D* within $CD100^+$ regions were similar (Figure 1*A* and *B*), indicating that CD100 at the transcriptional level was not different in PSC livers. The cholangiocyte marker CK19 (*KRT19*) was then used to define bile duct areas, and CD100 was more often colocalized to $CK19^+$ regions in PSC compared with non-PSC livers (Figure 1*C*), suggesting that $CD100^+$ immune cells preferentially localize around bile ducts in PSC.

The peribiliary localization of CD100 was not recapitulated at the protein level using immunohistochemistry, which revealed fewer $CD100^+$ stains in the PSC biliary regions compared with those of patients without PSC (Figure 1*D* and *E*). Even given the clear presence of $CD3^+$ T cells, a cell type supposed to express high levels of CD100, the $CD100^+$ signal was still poorly detected around the diseased bile ducts in patients with PSC (Figure 1*F* and *G*).

sCD100 was elevated in the plasma of donors with PSC compared with healthy donors and detected in the PSC bile samples (Figure 1*H*). However, controls without PSC had a similar or even more robust sCD100 increase in plasma and bile (Figure 1*I*). These results suggest that the cleavage of CD100 happens universally during liver inflammation and that the contradictory expression pattern of CD100 at transcriptomic and protein levels in PSC livers could potentially be explained by a mechanism that results in peribiliary CD100 cleavage.

Reduced Surface CD100 on Biliary Infiltrating Immune Cells

To closely assess CD100 expression on peribiliary immune cell subsets, we profiled leukocytes collected from ERCP brush samples by high-dimensional flow cytometry (Supplementary Figure 2*A*). Consistent with the diminished CD100 positive staining in situ, the overall surface CD100 expression was dramatically decreased on leukocytes ($CD45^+$) obtained from PSC bile ducts compared with PBMCs from matched blood samples (Figure 2*A* and *B*). A similar trend was also observed in the controls without PSC (Figure 2*B*). Among the biliary immune cells, CD100 was detected mainly on T and natural killer cells, but the expression level on these subsets was still much lower than that in PBMCs (Figure 2*C*). In absolute numbers, T cells were ~14-fold more abundant than natural killer cells (Supplementary Figure 3*A*) and thus the most likely source of sCD100. We also examined the presence of mast cells, which have been reported to be specifically recruited to the portal tracts in PSC livers[26,27] but detected very few of these cells in our samples (Supplementary Figure 4).

The decline in CD100 expression was more pronounced in CD4 T cells compared with CD8 T cells (Figure 2*D* and *E* and Supplementary Figure 3*B*). In line with previous observations,[21] the effector memory T cell (TEM, $CD45RA^-$C-C chemokine receptor type 7 [$CCR7]^-$) subset dominated the biliary T-cell population (Supplementary Figure 3*C*). CD4 and CD8 TEMs both markedly decreased CD100 expression in PSC bile ducts vs peripheral blood (Figure 2*F*, *top panel*), a similar but nonsignificant trend was observed in patients without PSC (Figure 2*F*, *bottom panel*). We also stained for

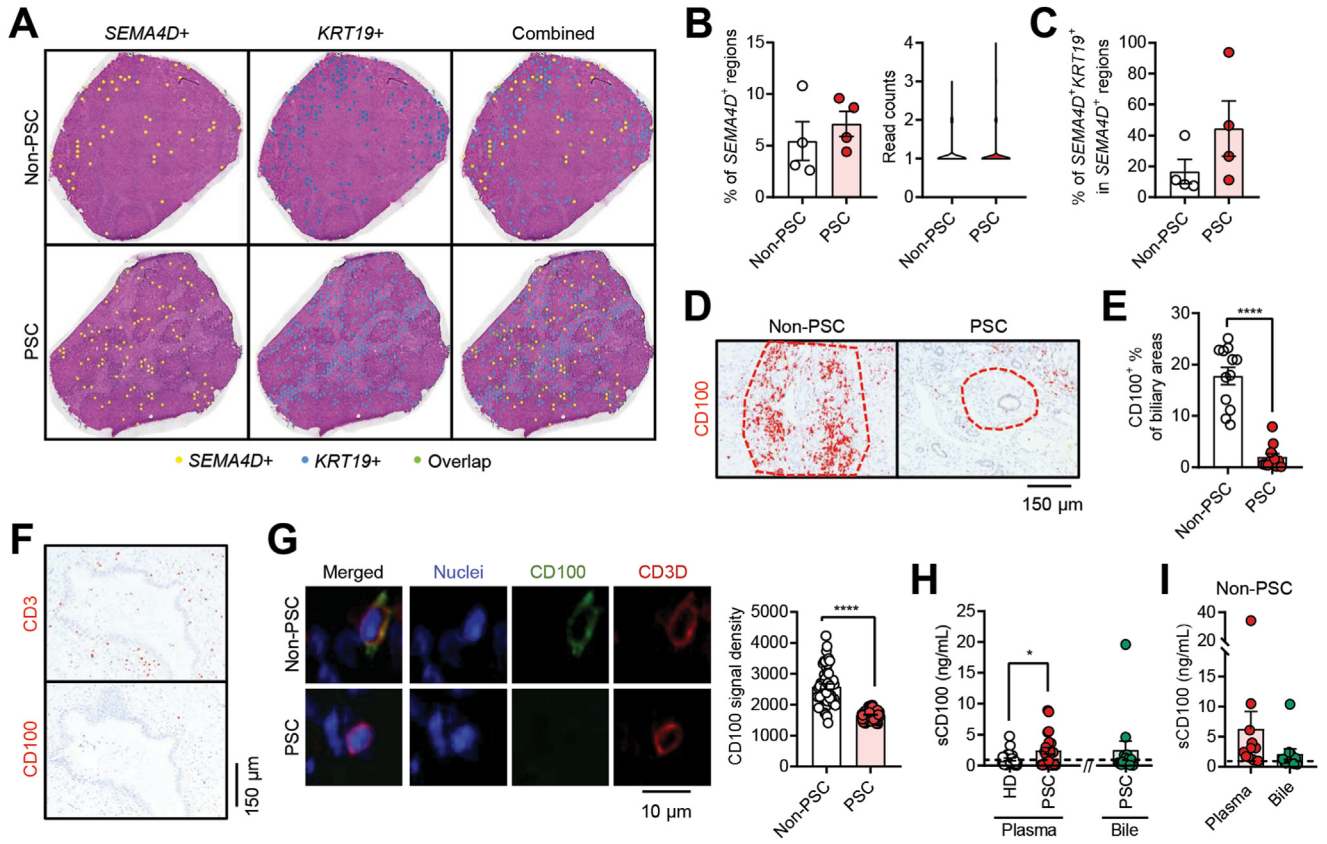

Figure 1. Local expression of CD100 in PSC livers. (*A*) Sequential 10-μm liver sections were obtained from PSC (n = 4) and non-PSC (n = 4) hilar core biopsies collected after liver transplantation. The section was used for spatial transcriptomics after H&E staining. Distribution of regions with CD100$^+$ cells (*SEMA4D*$^+$) and cholangiocytes (*KRT19*$^+$) was visualized by dots with indicated colors. (*B*) Quantification of CD100$^+$ regions (*left*) and the read counts of *SEMA4D,* the gene encoding CD100, within positive regions (*right*). (*C*) Quantification of regions with both CD100$^+$ cells and cholangiocytes. (*D*) Representative immunohistochemical staining and (*E*) quantification of CD100 in liver sections of PSC and non-PSC (original magnification ×100). Bar, 150 μm. Red, CD100$^+$. (*F*) Immunohistochemical images obtained from adjacent sections showing clear presence of CD3$^+$ T cells but poor CD100 expression at the diseased biliary area of PSC. Bar, 150 μm. Red, positive stain. (*G*) Immunofluorescence images illustrating that CD3 (red) and CD100 (green) were not coexpressed on the surface of a T cell adjacent to bile ducts in PSC. A T cell from non-PSC is shown as the positive control for CD100 staining. Statistical analysis comparing the CD100 signal density in T cells from a representative non-PSC to a representative PSC sample. Nuclei stained by 4′,6-diamidino-2-phenylindole, blue. Bar, 10 μm. (*H*) sCD100 levels in plasma and bile of patients with PSC (PSC plasma, n = 24; bile, n = 12) measured by enzyme-linked immunosorbent assay. Baseline (dashed line) was set by mean plasma sCD100 levels in healthy donors (HD, n = 23). (*I*) sCD100 levels in plasma and bile samples from non-PSC (n = 11). Statistical significance was determined using the unpaired *t* test. Data are presented as the mean ± standard error of the mean. *$P < .05$, ****$P < .0001$.

CD69, a marker for tissue-resident memory T cells,[28] and found that the expression of CD100 was comparable on biliary resident (CD69$^+$) and circulating (CD69$^-$) populations (Figure 2*G* and Supplementary Figure 3*D*). Together, these data further confirm reduced surface CD100 on biliary infiltrating immune cells, among which T cells are the dominant population.

CD100 Reduction After Pathogenic Cholangio-Immune Interaction

Bile duct dominance of the disease in patients carrying the CD100 mutation has suggested a pathogenic role of CD100 specifically affecting biliary sites. However, the markedly diminished surface CD100 on biliary immune cells indicates abolished CD100 signaling. To explain this apparent paradox, we hypothesized that CD100 cleavage is induced after the initiation of the local pathogenic immune responses. To test our hypothesis, we traced CD100 expression in a reductionistic coculture system, with ex vivo murine splenocytes, representing the recruited immune compartment and cholangiocyte cell lines mimicking the pathogenic immune responses at the biliary mucosal barrier.

After coculture of WT and CD100-mutated splenocytes with small or large cholangiocytes,[18] we observed a similar minor increase of cell death from 1% to 3% (Figure 3*A*) in both lines under unstimulated conditions. Upon stimulation and activation of the immune cells, the death rate increased specifically for large cholangiocytes and was more pronounced for the cocultures that included CD100-mutated splenocytes (Figure 3*B*), suggesting that this experimental

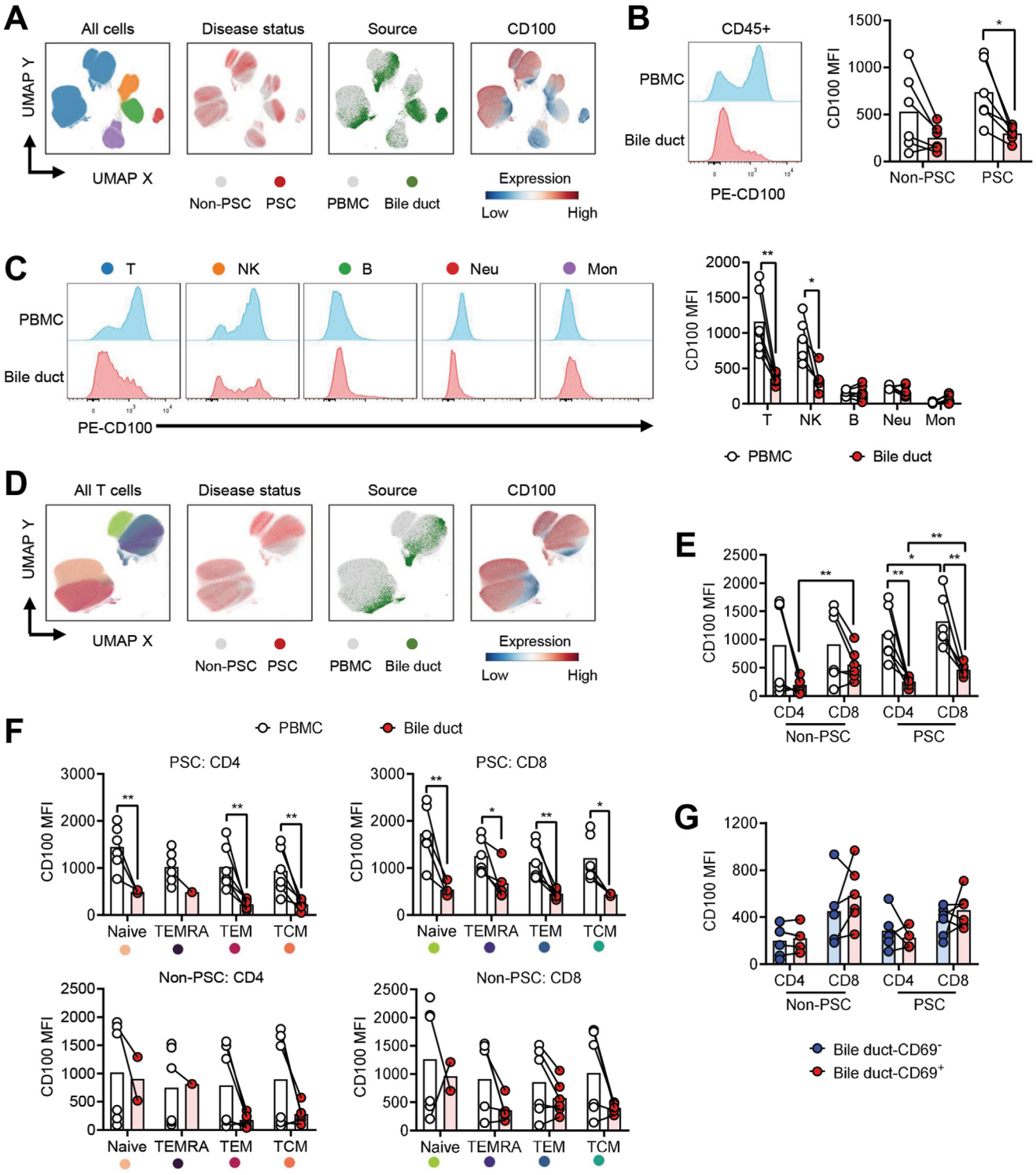

Figure 2. CD100 expression on biliary infiltrating immune cells. (*A*) UMAP plots of total CD45$^+$ cells stratified by disease status (PSC and non-PSC controls) and anatomical origin (PBMC or bile duct). The relative expression intensities of CD100 on total cells are also shown in the UMAP analysis. (*B*) Representative histogram and summary of median fluorescence intensity (MFI) showing surface CD100 expression on biliary infiltrating immune cells (bile duct) or PBMCs isolated from individuals with PSC (n = 6) or non-PSC (n = 6). (*C*) CD100 expression on biliary immune subsets of PSC. B, B cells; Mon, monocytes; Neu, neutrophils; NK, natural killer cells; T, T cells. The color pattern of each cell type is matched with what is shown in UMAP (all cells). (*D*) UMAP plots of total T cells and the relative expression intensities of CD100. (*E*) CD100 expression on CD4 and CD8 T-cell subsets. Unpaired *t* test was used for comparisons between CD4 and CD8 T cells. (*F*) CD100 expression on memory and naïve T cells. Naïve, naïve T cells (CD45RA$^+$ C-C chemokine receptor type 7 [CCR7]$^+$); TEMRA, T effector-memory cells with reacquired RA (CD45RA$^+$CCR7$^-$); TEM, effector memory T cells (CD45RA$^-$CCR7$^-$); TCM, central memory T cells (CD45RA$^-$CCR7$^+$). The color pattern of each subset is matched with what shown in UMAP (all T cells). (*G*) CD100 expression on biliary-resident (CD69$^+$) or circulating (CD69$^-$) T cells. If not otherwise stated, statistical significance was determined using the paired *t* test. *$P < .05$, **$P < .01$.

system seemingly recapitulates part of the immunopathology driven by the CD100 mutation. We also assessed senescence in cocultured cholangiocytes. Even though senescence was increased after coculture, there was no difference between the WT and mutated groups (Supplementary Figure 5).

Next, we examined whether the increased cell death was accompanied by reduced surface CD100 on cocultured immune cells ($CD45^+$). Indeed, a clear reduction was observed under both nonstimulated (Figure 3*C*) and anti-CD3/CD28–stimulated (Figure 3*D*) conditions when cocultured with large cholangiocytes. Cocultures with small cholangiocytes exhibited less reduction of CD100 (Figure 3*C* and *D*). Consistent with the observation in human biliary T cells, the CD100 reduction on CD4 T cells was more pronounced than on CD8 T cells (Figure 3*C* and *D*).

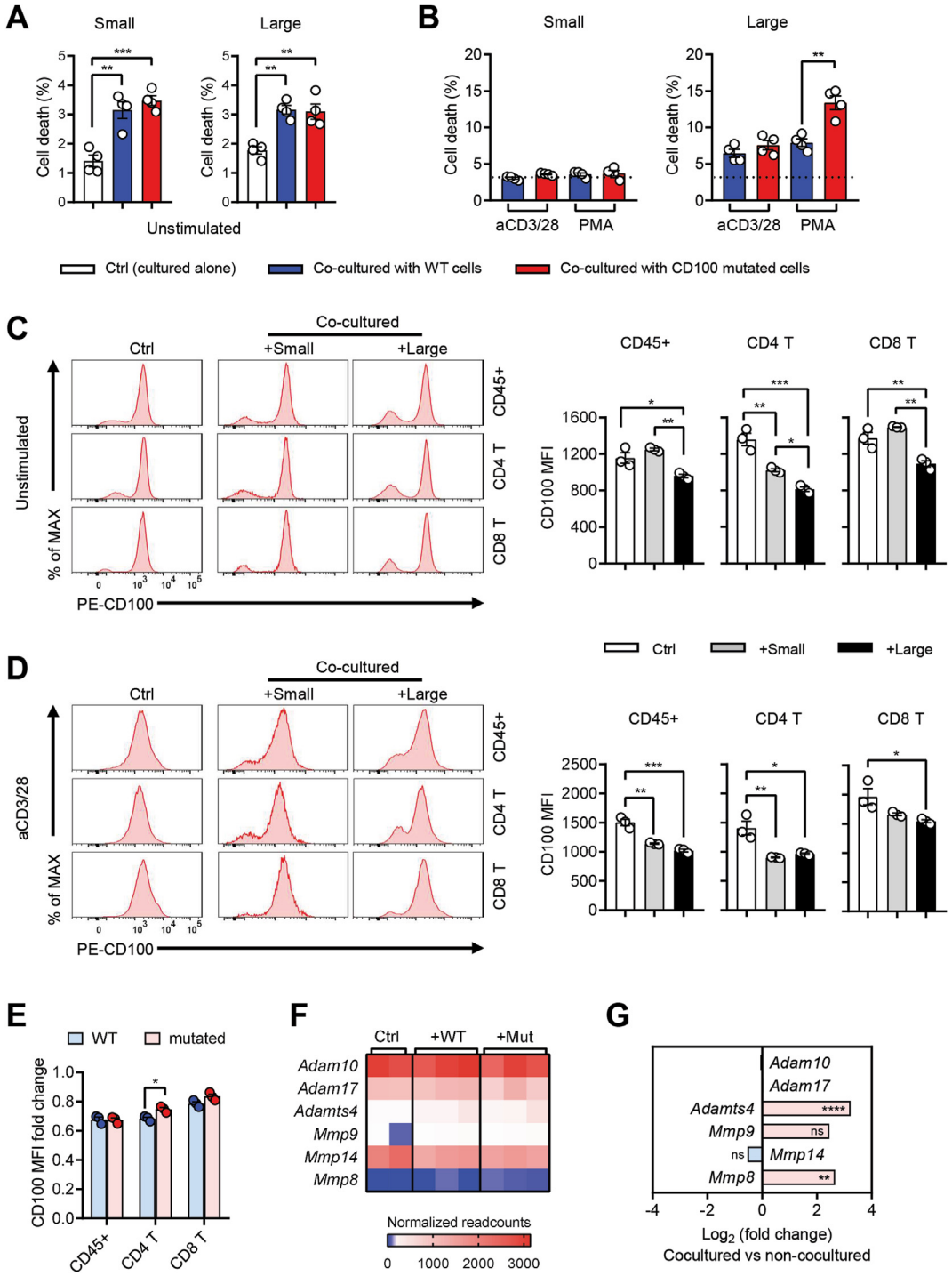

Nevertheless, CD100 was still retained at some levels on the surface of CD4 T-cell subsets at the time of harvest, and the expression was similar or slightly higher on mutated than WT cells (Figure 3*E*).

To evaluate whether MMP-induced cleavage is involved in the CD100 reduction, we performed RNA sequencing of the cocultured large cholangiocytes and analyzed the expression of MMPs that have been previously reported to cleave CD100.[9] *Adam10, Adam17,* and *Mmp14* were constitutively expressed in large cholangiocytes (Figure 3*F*), whereas *Adamts4* and *Mmp8* were markedly increased after coculturing with activated immune cells (Figure 3*G*). Thus, cholangiocyte-produced MMPs likely contribute to CD100 cleavage during pathogenic cholangio-immune interaction. Coculturing with WT and mutated cells had the same impact on MMP expression (Figure 3*F*). Taken together, these findings suggest that the peribiliary-specific CD100 reduction in PSC livers can be a consequence of feedback regulation driven by cholangiocytes that are under immune attack.

Skewed T-Helper 17 Cell Differentiation in Cholangiocyte-Adherent T Cells

The coculture system recapitulating the pathogenic cholangiocyte-immune cell interaction also allowed us to perform in-depth mechanistic assessments. We consistently observed a group of immune cells adherent to cholangiocytes along with immune cells floating in the cell culture media (nonadherent), and the proportion of adherent immune cells was further increased upon immune cell stimulation (Supplementary Figure 6*A*). The CD100-mutated immune cells cultured with large cholangiocytes had a higher propensity to adhere when they were stimulated (Supplementary Figure 6*A*). When all conditions were analyzed together, we observed a strong linear relationship between the death rate of cholangiocytes and abundance of adherent immune cells (Supplementary Figure 6*B*). This phenomenon suggests that the adherent immune cells are likely to be pathogenic, and we found that T cells were enriched in this layer (Supplementary Figure 6*C*).

To examine the functional alterations of cholangiocyte-adherent T cells, we purified T cells from the adherent layer (adherent T) and the coculture suspension (nonadherent T), respectively, for bulk RNA sequencing (Figure 4*A*). The gene expression profile was notably altered in adherent T cells compared with nonadherent T cells that were exposed to the identical culture environment. We identified 2880 up-regulated genes in adherent T cells and 1615 down-regulated genes (cutoff: P value $< .05$, $|\log_2 \text{foldchange}| > 0$) (Figure 4*B*).

KEGG pathway analysis of the differentially expressed genes identified markedly dysregulated pathways of relevance to bile duct inflammation (Figure 4*C*). The up-regulated genes of the apoptosis pathways ($P < 1.0E{-}6$) in adherent T cells encode growth factors and antiapoptosis proteins, such as *Bcl2a1a* and *Bcl2a1d* (Figure 4*D*). Also, *Tnf, Gzmb,* and *Fasl,* which are involved in cytotoxicity functions, were up-regulated in adherent T cells (Figure 4*D*). These findings suggest that the adherent T cells are protected from apoptosis and more cytotoxic.

Several cytokine-related pathways were also identified, among which T-helper 17 (Th17) cell differentiation ($P < .005$) is of particular interest because pronounced Th17 cells have been reported in PSC livers.[29,30] Detailed examination of candidate genes in the Th17 cell differentiation pathway revealed that Th17-related cytokines were up-regulated in adherent T cells, including *Ifng, Il17a, Il17f,* and *Il22* (Figure 4*E*). In addition, the increased expression level of *Il23r* on T cells further supports the pathogenicity of induced Th17 cells in the adherent layer (Figure 4*E*), because interleukin (IL) 23 has a critical role in endowing Th17 cells with pathogenic effector function.[31] These changes were accompanied by an altered IL17 signaling pathway in cholangiocytes from the same culture, featured by *Il1β* and *Il6,* 2 cytokines known to drive Th17 differentiation in PSC,[32] and by Th17-related chemokines including *Cxcl2, Cxcl10, Ccl11*, and *Ccl20* (Figure 4*F*). *Il17rc,* the gene that encodes the receptor for IL17A and IL17F, also showed higher expression in cholangiocytes after coculture (Figure 4*F*).

Figure 3. Coculture with cholangiocytes leads to CD100 reduction on T-cell surface. (*A*) Small or large cholangiocytes were cultured alone or cocultured with splenocytes from WT and CD100 mutated mice without additional stimulation. The death rate of cholangiocytes was accessed by dead cell marker stain and examined by flow cytometry (n = 4; means ± standard error of the mean). Small, small cholangiocytes; Large, large cholangiocytes. (*B*) The frequency of dead cholangiocytes was analyzed after coculturing with activated immune cells. Indicated stimuli were added into the coculture. aCD3/28, soluble anti-CD3 and anti-CD28; PMA, phorbol myristate acetate mixed with ionomycin. The dotted line indicates the average death rate under unstimulated conditions. Significance was calculated by unpaired *t* tests. (*C*) Representative histogram and summary of CD100 expression on total immune cells (alive $CD45^+$ cells), CD4, and CD8 T cells in unstimulated coculture. Ctrl, cultured alone; +Small, cocultured with small cholangiocytes; +Large, cocultured with large cholangiocytes. WT cells were used (n = 3). (*D*) Representative histogram and summary of CD100 expression on total immune cells, CD4 and CD8 T cells in the coculture with aCD3/28. WT cells were used (n = 3). (*E*) CD100 expression was compared in WT (n = 3) and mutated immune cells (n = 3) after coculturing with large cholangiocytes in the presence of aCD3/28. Fold change was calculated by normalizing to average CD100 median fluorescence intensity (MFI) under unstimulated conditions. Significance was calculated by unpaired *t* tests. (*F*) Heat map showing normalized read counts of MMPs in cocultured large cholangiocytes (RNA sequencing data, n = 2–3). Ctrl, large cholangiocytes cultured alone; +WT, cocultured with WT immune cells; +Mut, cocultured with mutated immune cells. (*G*) Statistical analysis of gene expression in *F*. Fold change (normalized to Ctrl) and adjusted *P* value were calculated by DESeq2 (Bioconductor). Red, up-regulated after coculture; blue, down-regulated after coculture. Experiments were repeated at least twice. Statistical significance was determined using 1-way analysis of variance tests, followed by Bonferroni's correction if not specifically indicated. ns, not significant; $^*P < .05$, $^{**}P < .01$, $^{***}P < .001$, $^{****}P < .0001$.

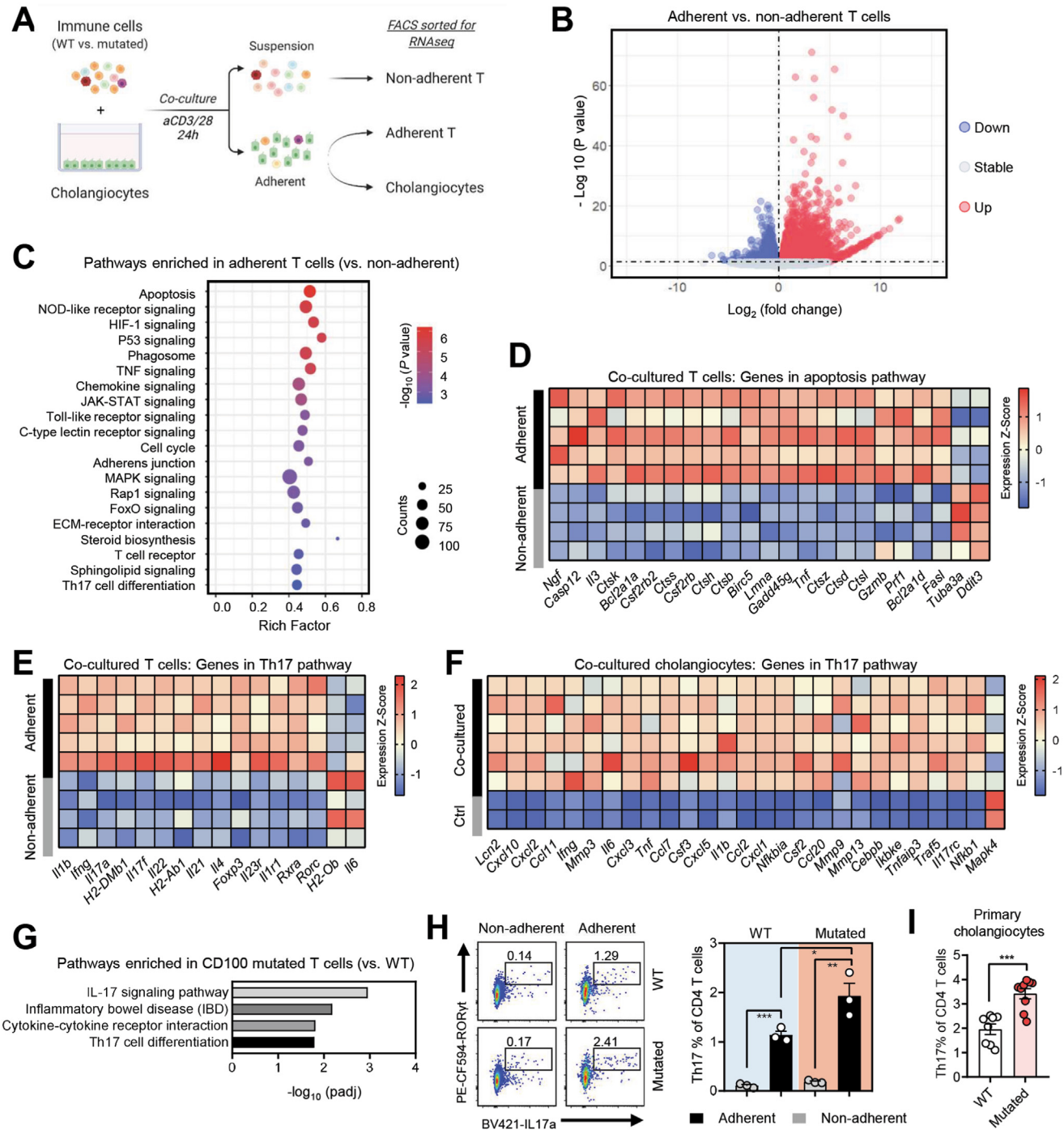

Figure 4. Cholangiocyte-adherent T cells are protected from apoptosis and biased to Th17 differentiation. (*A*) Workflow showing the procedure of coculture and the preparation of cells used for bulk RNA sequencing. Immune cells isolated from the spleen of WT or CD100 mutated mice were cocultured with large cholangiocytes. aCD3/28, stimulated by anti-CD3 and anti-CD28. (*B*) Differential gene expression between nonadherent and adherent T cells. Up genes, red; down genes, blue; stable genes, gray. Data generated from biological repeats (nonadherent T cells, n = 4; adherent T cells, n = 5) were included in the analysis. (*C*) KEGG terms that were enriched among differentially expressed genes in adherent T cells. ECM, extracellular matrix; HIF-1, hypoxia-inducible factor 1; JAK/STAT, Janus kinase/signal transducer and activator of transcription proteins; MAPK, mitogen-activated protein kinase; NOD, nucleotide-binding oligomerization domain; TNF, tumor necrosis factor. (*D*) Heat map showing the expression level of altered genes in apoptosis-related pathway between nonadherent and adherent T cells. (*E*) Heat map showing the expression level of altered genes in the Th17 cell differentiation pathway between nonadherent and adherent T cells. (*F*) Heat map comparing the expression signal of genes in the IL17 signaling pathway in cocultured large cholangiocytes vs controls that were cultured alone (Ctrl). (*G*) KEGG terms that were enriched among differentially expressed genes in CD100 mutated T cells. padj, adjusted *P* value. (*H*) Dot plots and statistical analysis of Th17 cells (RORγt^{+}IL17A^{+}) in nonadherent and adherent CD4 T cells after coculture with large cholangiocytes. WT (n = 3) and CD100 mutated T cells (n = 3) were compared to show the impact of the CD100 mutation on Th17 differentiation. (*I*) Th17 cells in adherent CD4 T cells after coculture with murine primary cholangiocytes (n = 8–9). Experiments were repeated at least twice. Data are presented as the mean ± standard error of the mean. Statistical significance was determined using unpaired *t* tests. *$P < .05$, **$P < .01$, ***$P < .001$.

When the CD100-mutated T cells were compared with WT T cells isolated from the adherent layer, we observed further enrichment of the IL17 signaling and Th17 cell differentiation pathways in mutated T cells (Figure 4*G*). These findings were also evident on the protein level because the proportion of Th17 T cells ($CD4^+$ retinoic acid-related orphan receptor -γ [RORγt]$^+$IL17A$^+$) was higher in adherent than in nonadherent CD4 T cells and further increased in the CD100-mutated group when assessed with flow cytometry (Figure 4*H* and Supplementary Figure 2*B*). We also observed an increase of Th17 cells among mutated immune cells when cocultured with primary cholangiocytes (Figure 4*I*).

The production of IL1β and IL6 were similar in cholangiocytes cocultured with WT or mutated cells in the presence of aCD3/CD28, implying the further skewed Th17 differentiation in mutated T cells is less likely to be cytokine-dependent (Supplementary Figure 7). Collectively, the data presented here suggest that cholangiocyte-immune cell cross talk facilitates the pathogenic Th17 cell differentiation and that the CD100 causal mutation can boost this process.

T-Helper 17 Cells Dominate Biliary-Resident CD4 T Cells in Patients

Based on the murine coculture experiments suggesting Th17 differentiation driven by cholangiocyte-immune interaction, we reasoned that T cells in the bile ducts of humans would also display a Th17-enriched phenotype, especially among tissue-resident CD4 T cells. Therefore, we examined the Th17 proportion in leukocytes isolated from ERCP samples.

To overcome the challenges in continuous RORγt staining and phenotype alteration during the stimulation for IL17A detection, we decided to use the marker CD161 for Th17 characterization[33] and excluded other CD4 T-cell populations that might express CD161 by TCR-Va7.2 (for MAIT cells) and T-bet (for Th1 cells). Also, because of the TEM dominance among biliary CD4 T cells, we specifically compared the percentage of Th17 cells of TEM in PBMC and bile duct to rule out the potential impacts caused by naïve/memory status. Indeed, the Th17 proportion of CD4 TEM was much higher in bile duct than PBMC in both PSC and non-PSC samples (Figure 5*A*). Biliary Th17 cells also displayed distinct phenotype compared with their PBMC counterparts, such as decreased CD100 and increased tissue-resident marker CD69 (Figure 5*A*). Cytokine production assays confirmed these cells were more potent to secrete IL17A (Figure 5*B*).

We then zoomed into tissue-resident ($CD69^+$) T cells and found they express higher RORγt (Figure 5*C*), which is consistent with the findings in the murine system. The percentage of Th17 cells was much higher in biliary-resident ($CD69^+$) than biliary-circulating ($CD69^-$) cells (Figure 5*D*). We also observed that biliary-resident Th17 cells produced comparable IL17A as biliary-circulating Th17 cells but more IL2 and tumor necrosis factor (Figure 5*E*), implying enhanced pathogenicity. Thus, we confirm that Th17 cells are dominating biliary-resident CD4 T cells in human livers with PSC or non-PSC cholangiopathies.

Discussion

The present study suggests that CD100 exerts its functional impact in bile duct inflammation through cholangiocyte-immune cell cross talk and underscores an active, proinflammatory role of cholangiocytes. The CD100 mutation is here involved in a previously undescribed biliary-specific pathogenic process in which cholangiocytes facilitate interacted CD4 T cells to undergo pathogenic Th17 differentiation. Also, immune-challenged cholangiocytes can shape local CD100 expression likely by up-regulating MMPs to cleave surface CD100 from biliary infiltrating immune cells, serving as a feedback response to immune insults. Similar phenotypes, including cholangiocyte-driven Th17 differentiation and reduced peribiliary CD100 expression, are also present in diseased livers of patients with cholangiopathies but not carrying the mutation. Therefore, our findings have identified important key biliary-specific cellular players and pathogenic processes that CD100 is involved in, which are likely to have implications for biliary inflammation in general.

Increased Th17 differentiation in vivo and prominent IL17 responses to microbial stimulation have been reported in patients with PSC.[29,32] In the previously raised theory, the differentiation of Th17 cells is driven by microbe-stimulated monocytes, and these cells are then recruited to portal areas by cholangiocyte-produced chemokines.[32] Herein, we describe a distinct and complementary mechanism in which Th17 cells are locally differentiated due to their interaction with cholangiocytes.

In our reductionistic experiments, we cocultured cholangiocytes together with T cells, leading to Th17 cell lineage bias. This is an interesting observation in general because differentiation of T cells into helper cell lineages is a complicated process contingent on numerous variable factors,[34,35] whereas our data showed that cholangiocytes appear to provide sufficient signaling for Th17 lineage. Our results suggest a programmed fate decision for T cells after interaction with cholangiocytes, which may advance the understanding of bile duct local immunity and immune-driven biliary diseases. This notion is in line with the recent discovery of a population of liver-resident naïve T cells that have a propensity to acquire Th17-associated effector functions in PSC livers.[30]

Our findings underscore an active, pathogenic role of cholangiocytes in PSC progression. The signals provided by these cells and the feedback responses mounted by them, such as Th17 differentiating signals and MMPs that cleave CD100 and generate proinflammatory sCD100, can actually exacerbate the overall pathogenic inflammation. This concept could partly explain the fact that immunosuppressive treatments that lower the magnitude of pathogenic immune activities show poor efficacy in PSC patients,[36,37] referred to as the immune paradox of PSC.[38] Treatment approaches combining inhibition of established inflammation and termination of cholangiocyte-driven pathogenic factors could be a way forward. A role for cholangiocyte-immune cross talk in promoting Th17 survival and expansion was previously reported in PBC, but the mechanisms described were through soluble factors[39] and thus could not

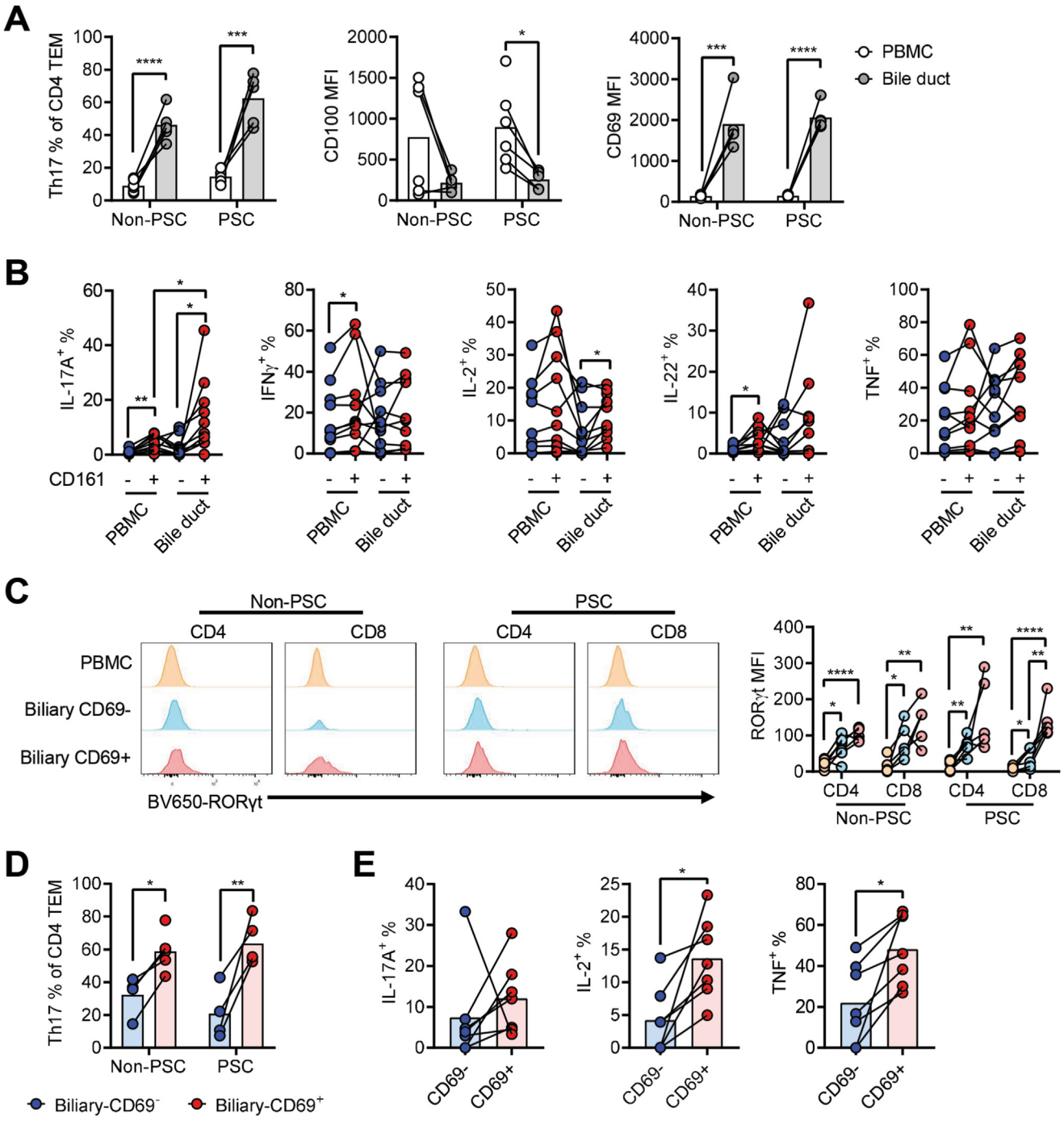

Figure 5. Th17 cells are dominant in tissue-resident CD4 TEM cells from patients with inflamed bile ducts. (*A*) Proportion of Th17 (Va7.2^{-}T-bet^{-}CD4^{+}CD161^{+} TEM) cells and their surface expression of CD100 and CD69 in PBMC and ERCP brush samples (non-PSC, n = 6; PSC, n = 6). MFI, median fluorescence intensity. (*B*) The cytokine production capacity of Th17 cells after stimulation with phorbol myristate acetate and ionomycin in patients with PSC. IFN, interferon; TNF, tumor necrosis factor. (*C*) Representative histogram and statistical analysis showing that the biliary-resident (CD69^{+}) T cells express higher RORγt than biliary-circulating (CD69^{-}) and PBMC T cells. (*D*) Proportion of Th17 (Va7.2^{-}T-bet^{-}CD4^{+}CD161^{+} TEM) cells in biliary resident and circulating CD4 TEMs. (*E*) Cytokine production from biliary resident or circulating Th17 cells after phorbol myristate acetate and ionomycin stimulation. Statistical significance was determined using paired or unpaired *t* tests or Mann-Whitney or Wilcoxon's signed rank tests. *$P < .05$, **$P < .01$, ***$P < .001$, ****$P < .0001$.

explain the Th17 observations in only cholangiocyte-adherent while not in suspension T cells in this study. Understanding and manipulating the surface molecular pairs that mediate pathogenic cholangiocyte-immune cell interaction may provide new approaches to mitigate biliary inflammation in the future.

This study provides an explanation about how the CD100 mutation causes biliary-specific disease, but very limited

CD100 protein expression can be detected at the diseased site. Our data suggest that decreased CD100 on biliary infiltrating immune cells is a feedback response driven by immune-challenged cholangiocytes. The mutation would still be functional at the initial phase of immunopathology because the cleavage takes time and the pathogenic differentiation can be established during CD100 reduction. In the current study, we aimed to understand the pathogenic role of the CD100 causal mutation, so our focus was more on the inflammation-triggering or early-disease phase, or both. Despite a mechanism through T cells described here, we cannot formally rule out the possibility that the CD100 signals have additional roles through other cell types in later stages, such as mast cells, which are found in bile duct areas in fibrotic PSC livers.[26,27]

The CD100-plexin B2 interaction promotes tissue healing in the skin and colon,[40,41] so the cleavage of CD100 may also contribute to biliary local inflammation by abolishing these protective effects and generating proinflammatory sCD100. That sCD100 can promote IL17 and IL22 production in T cells has been shown.[42] This effect appears to be minor in our coculture system, because only T cells adherent to cholangiocyte were biased to Th17 differentiation but not the T cells in the suspension, despite the identical culture environment. Thus, we assume that the interaction with cholangiocytes provides much stronger or additional Th17 differentiation signals to T cells than sCD100. Because Th17-related pathways are more pronounced in mutated than in WT T cells and there was no difference in cholangiocyte-secreted IL1β and IL6 in our experimental system, the signal enhanced by the CD100 mutation likely facilities Th17 development.

Conclusion

Although detailed molecular mechanisms remain to be defined, the impact of cholangiocytes on pathogenic Th17 cells is remarkable and highlights an active role of cholangiocytes in PSC pathogenesis. Our findings also link the CD100 mutation to Th17, which is a shared phenotype seen in patients with PSC not carrying the mutation. This opens the possibility of using mutation-specific tools to identify key molecules at the core of pathogenic cholangiocyte-immune cell interaction as general treatment targets for biliary inflammation.

Supplementary Material

Note: To access the supplementary material accompanying this article, visit the online version of *Gastroenterology* at www.gastrojournal.org, and at https://doi.org/10.1053/j.gastro.2023.11.283.

References

1. Claussnitzer M, Cho JH, Collins R, et al. A brief history of human disease genetics. Nature 2020;577:179–189.
2. Peltonen L, Perola M, Naukkarinen J, et al. Lessons from studying monogenic disease for common disease. Hum Mol Genet 2006;15(Spec No 1):R67–R74.
3. Jiang X, Bergquist A, Loscher BS, et al. A heterozygous germline CD100 mutation in a family with primary sclerosing cholangitis. Sci Transl Med 2021;13:eabb0036.
4. Hirschfield GM, Karlsen TH, Lindor KD, et al. Primary sclerosing cholangitis. Lancet 2013;382:1587–1599.
5. Lazaridis KN, LaRusso NF. Primary sclerosing cholangitis. N Engl J Med 2016;375:1161–1170.
6. Dyson JK, Beuers U, Jones DEJ, et al. Primary sclerosing cholangitis. Lancet 2018;391:2547–2559.
7. Kikutani H, Kumanogoh A. Semaphorins in interactions between T cells and antigen-presenting cells. Nat Rev Immunol 2003;3:159–167.
8. Kumanogoh A, Kikutani H. Immunological functions of the neuropilins and plexins as receptors for semaphorins. Nat Rev Immunol 2013;13:802–814.
9. Wang L, Li X, Song Y, et al. The emerging roles of semaphorin4D/CD100 in immunological diseases. Biochem Soc Trans 2020;48:2875–2890.
10. Bougeret C, Mansur IG, Dastot H, et al. Increased surface expression of a newly identified 150-kDa dimer early after human T lymphocyte activation. J Immunol 1992;148:318–323.
11. Zhang Y, Cao H, Chen J, et al. Adiponectin-expressing Treg facilitate T lymphocyte development in thymic nurse cell complexes. Commun Biol 2021;4:344.
12. Delaire S, Elhabazi A, Bensussan A, et al. CD100 is a leukocyte semaphorin. Cell Mol Life Sci 1998;54:1265–1276.
13. Yoshida Y, Ogata A, Kang S, et al. Semaphorin 4D contributes to rheumatoid arthritis by inducing inflammatory cytokine production: pathogenic and therapeutic implications. Arthritis Rheumatol 2015;67:1481–1490.
14. Nishide M, Nojima S, Ito D, et al. Semaphorin 4D inhibits neutrophil activation and is involved in the pathogenesis of neutrophil-mediated autoimmune vasculitis. Ann Rheum Dis 2017;76:1440–1448.
15. Maleki KT, Cornillet M, Bjorkstrom NK. Soluble SEMA4D/CD100: a novel immunoregulator in infectious and inflammatory diseases. Clin Immunol 2016;163:52–59.
16. Murakami T, Takahata Y, Hata K, et al. Semaphorin 4D induces articular cartilage destruction and inflammation in joints by transcriptionally reprogramming chondrocytes. Sci Signal 2022;15:eab15304.
17. **Tysoe OC**, **Justin AW**, **Brevini T**, et al. Isolation and propagation of primary human cholangiocyte organoids for the generation of bioengineered biliary tissue. Nat Protoc 2019;14:1884–1925.
18. Ueno Y, Alpini G, Yahagi K, et al. Evaluation of differential gene expression by microarray analysis in small and large cholangiocytes isolated from normal mice. Liver Int 2003;23:449–459.
19. Chung BK, Ogaard J, Reims HM, et al. Spatial transcriptomics identifies enriched gene expression and cell types in human liver fibrosis. Hepatol Commun 2022;6:2538–2550.
20. Schindelin J, Arganda-Carreras I, Frise E, et al. Fiji: an open-source platform for biological-image analysis. Nat Methods 2012;9:676–682.
21. Zimmer CL, von Seth E, Buggert M, et al. A biliary immune landscape map of primary sclerosing cholangitis

reveals a dominant network of neutrophils and tissue-resident T cells. Sci Transl Med 2021;13:eabb3107.
22. Becht E, McInnes L, Healy J, et al. Dimensionality reduction for visualizing single-cell data using UMAP. Nat Biotechnol 2019;37:38–44.
23. Anders S, Huber W. Differential expression analysis for sequence count data. Genome Biol 2010;11:R106.
24. Yu G, Wang LG, Han Y, et al. clusterProfiler: an R package for comparing biological themes among gene clusters. OMICS 2012;16:284–287.
25. Racanelli V, Rehermann B. The liver as an immunological organ. Hepatology 2006;43:S54–S62.
26. **Jones H**, **Hargrove L**, Kennedy L, et al. Inhibition of mast cell-secreted histamine decreases biliary proliferation and fibrosis in primary sclerosing cholangitis Mdr2$^{-/-}$ mice. Hepatology 2016;64:1202–1216.
27. Gonzalez MI, Vannan DT, Eksteen B, et al. Mast cells in immune-mediated cholangitis and cholangiocarcinoma. Cells 2022;11:375.
28. Kumar BV, Ma W, Miron M, et al. Human tissue-resident memory T cells are defined by core transcriptional and functional signatures in lymphoid and mucosal sites. Cell Rep 2017;20:2921–2934.
29. Katt J, Schwinge D, Schoknecht T, et al. Increased T helper type 17 response to pathogen stimulation in patients with primary sclerosing cholangitis. Hepatology 2013;58:1084–1093.
30. Poch T, Krause J, Casar C, et al. Single-cell atlas of hepatic T cells reveals expansion of liver-resident naive-like CD4(+) T cells in primary sclerosing cholangitis. J Hepatol 2021;75:414–423.
31. Wu C, Yosef N, Thalhamer T, et al. Induction of pathogenic T_H17 cells by inducible salt-sensing kinase SGK1. Nature 2013;496:513–517.
32. Kunzmann LK, Schoknecht T, Poch T, et al. Monocytes as potential mediators of pathogen-induced T-helper 17 differentiation in patients with primary sclerosing cholangitis (PSC). Hepatology 2020;72:1310–1326.
33. Annunziato F, Cosmi L, Liotta F, et al. Defining the human T helper 17 cell phenotype. Trends Immunol 2012;33:505–512.
34. Bhaumik S, Basu R. Cellular and molecular dynamics of Th17 differentiation and its developmental plasticity in the intestinal immune response. Front Immunol 2017;8:254.
35. Wang X, Ni L, Wan S, et al. Febrile temperature critically controls the differentiation and pathogenicity of T helper 17 cells. Immunity 2020;52:328–341.e5.
36. Goode EC, Rushbrook SM. A review of the medical treatment of primary sclerosing cholangitis in the 21st century. Ther Adv Chronic Dis 2016;7:68–85.
37. Vesterhus M, Karlsen TH. Emerging therapies in primary sclerosing cholangitis: pathophysiological basis and clinical opportunities. J Gastroenterol 2020;55:588–614.
38. Hov JR, Karlsen TH. The microbiota and the gut-liver axis in primary sclerosing cholangitis. Nat Rev Gastroenterol Hepatol 2023;20:135–154.
39. Jeffery HC, Hunter S, Humphreys EH, et al. Bidirectional cross-talk between biliary epithelium and Th17 cells promotes local Th17 expansion and bile duct proliferation in biliary liver diseases. J Immunol 2019;203:1151–1159.
40. Witherden DA, Watanabe M, Garijo O, et al. The CD100 receptor interacts with its plexin B2 ligand to regulate epidermal $\gamma\delta$ T cell function. Immunity 2012;37:314–325.
41. Meehan TF, Witherden DA, Kim CH, et al. Protection against colitis by CD100-dependent modulation of intraepithelial $\gamma\delta$ T lymphocyte function. Mucosal Immunol 2014;7:134–142.
42. Xie J, Wang Z, Wang W. Semaphorin 4D Induces an imbalance of Th17/Treg cells by activating the aryl hydrocarbon receptor in ankylosing spondylitis. Front Immunol 2020;11:2151.

Author names in bold designate shared co-first authorship.

Received February 28, 2023. Accepted November 8, 2023.

Correspondence
Address correspondence to: Espen Melum, MD, PhD, Oslo University Hospital, Postboks 4950 Nydalen, 0424 Oslo, Norway. e-mail: espen.melum@medisin.uio.no.

Acknowledgments
The authors thank Anne Pharo, Enya Amundsen-Isaksen, and the flow cytometry core facility at Oslo University Hospital for experimental assistance, and thank Anna Frank at Oslo University Hospital for valuable scientific input and Hong Qu at the Institute of Basic Medical Sciences, University of Oslo, for slide scanning. The authors also thank Kari C. Toverud for the liver illustration in the graphical abstract.

CRediT Authorship Contributions
Xiaojun Jiang, PhD (Conceptualization: Lead; Data curation: Lead; Formal analysis: Lead; Investigation: Lead; Methodology: Lead; Writing – original draft: Lead)
Kari Otterdal, PhD (Data curation: Supporting; Formal analysis: Supporting; Investigation: Supporting; Methodology: Supporting)
Brian K. Chung, PhD (Formal analysis: Supporting; Resources: Supporting; Visualization: Supporting)
Christopher Maucourant, PhD (Data curation: Supporting; Methodology: Supporting)
Jørgen D. Rønneberg, MSc (Data curation: Supporting; Formal analysis: Supporting; Methodology: Supporting)
Christine L. Zimmer, PhD (Data curation: Supporting; Formal analysis: Supporting)
Jonas Øgaard, BSc (Formal analysis: Supporting; Methodology: Supporting)
Yuliia Boichuk, MSc (Investigation: Supporting; Methodology: Supporting)
Sverre Holm, PhD (Data curation: Supporting; Methodology: Supporting)
Daniel Geanon, BSc (Formal analysis: Supporting; Visualization: Supporting)
Georg Schneditz, PhD (Formal analysis: Supporting; Methodology: Supporting; Supervision: Supporting)
Annika Bergquist, MD, PhD (Resources: Supporting)
Niklas K. Björkström, MD, PhD (Supervision: Supporting; Writing – review & editing: Supporting)
Espen Melum, MD, PhD (Funding acquisition: Lead; Project administration: Lead; Supervision: Lead; Writing – review & editing: Lead)

Conflicts of interest
The authors disclose no conflicts.

Funding
This work was supported by the Research Council of Norway (grant no. 325435) and the Norwegian PSC Research Center.

Data Availability
Bulk RNA sequencing data have been deposited into the National Center for Biotechnology Information (NCBI) Sequence Read Archive (SRA) database, under BioProject accession PRJNA1029520 (https://www.ncbi.nlm.nih.gov/bioproject/PRJNA1029520).